MASS TRANSFER INSIDE A FLUX HOOD FOR THE SAMPLING OF GASEOUS EMISSIONS FROM LIQUID SURFACES – AN EXPERIMENTAL ASSESSMENT

Ademir A. Prata Jr[a], Federico Lucernoni[b], Jane M. Santos[c], Laura Capelli[b], Selena Sironi[b], Nhat Le-Minh[a], Richard M. Stuetz[a,*]

[a]*UNSW Water Research Centre, School of Civil and Environmental Engineering, The University of New South Wales, Sydney, NSW, 2052, Australia*

[b] *Politecnico di Milano, Department of Chemistry, Materials and Chemical Engineering "Giulio Natta" - Piazza L. da Vinci 32, 20133 Milano, Italy*

[c]*Departamento de Engenharia Ambiental, Universidade Federal do Espírito Santo, Av. Fernando Ferrari 514, 29.060-970, Vitória, ES, Brazil*

*Corresponding Author: +61 (0)2 9385 5944; Email: r.stuetz@unsw.edu.au.

ABSTRACT

This study assesses the mass transfer of compounds inside the US EPA flux hood, one of the enclosure devices most commonly employed for the direct measurement of atmospheric emissions from liquid surfaces in wastewater treatment plants (WWTPs). Experiments comprised the evaporation of water and the volatilisation of a range of volatile organic compounds (VOCs). Special attention was given to the evaluation of the mass transfer coefficients in the microenvironment created by the flux hood and the effects of concentration build up in the hood`s headspace. The VOCs emission rates and the water evaporation rates generally increased with the sweep air flow rate, as did the mass transfer coefficients for all compounds. The emission of compounds whose volatilisation is significantly influenced by the gas phase was greatly affected by concentration build up, whereas this effect was not significant for liquid phase-controlled compounds. The gas-film mass transfer coefficient (k_G) estimated inside the US EPA flux hood was of the same order as the respective k_G reported in the literature for wind tunnel-type devices, but the emission rates measured by the flux hood can be expected to be lower, due to the concentration build-up. Compared against an emission model for the passive surfaces in WWTPs, the mass transfer of gas phase-dominated compounds inside the US EPA flux hood was equivalent to conditions of very low wind speeds. A procedure is presented in order to scale the emission rates of these compounds measured with the flux hood to field conditions of higher winds.

Keywords: dynamic flux chamber, odour emission, area sources, mass transfer coefficients

1. INTRODUCTION

In wastewater treatment plants (WWTPs), compounds emitted from liquid surfaces to the atmosphere are potential sources of environmental impacts, commonly due to offensive odours that cause annoyance to the exposed communities (Capelli et al., 2009b; Nicell, 2009; Hayes et al., 2014). The determination of the emission rate of odours or odorous compounds from liquid surfaces is then critical for the study and management of such impacts (Bluden and Aneja, 2008; Latos et al., 2011; Rumsey et al., 2012). The so-called passive liquid surfaces (i.e., surfaces without an active gas flow, such as mechanical aeration or intense bubbling), for instance primary and secondary settlement tanks, sequencing batch reactors and stabilisation ponds, are major sources of odorous emissions in WWTPs. The accurate determination of emission rates for this type of surfaces is particularly challenging, and different approaches have been proposed, which can be divided into the following groups (Gostelow et al., 2001b, 2003; Hudson and Ayoko, 2008b; Santos et al., 2012):

- Using predictive emission models, which contain empirical correlations to estimate emission rates of individual compounds. Alternatively, if a simpler and rough estimate of the overall odour emission rate (in odour units per unit time) is desired, Odour Emission Factors (Capelli et al., 2009a) can be applied.
- Applying reverse dispersion modelling (indirect method) to back calculate the emission rate based on environmental concentrations measured around the source (see examples in Latos et al., 2011, Grant et al., 2013, and Schauberger et al., 2013).
- Using an enclosure device (direct methods) to sample emissions directly at the surface.

Direct method have been more broadly adopted for the assessment of emissions at surfaces (e.g., Muezzinoglu, 2003; Blunden and Aneja, 2008; Beghi et al., 2012; Rumsey et al., 2012; Hentz et al., 2013; Parker et al., 2013a; Xiao et al., 2014) due to being less costly and easier to handle (Hudson and

Ayoko, 2008b; Capelli et al., 2013). Two groups are identified (Hudson and Ayoko, 2008b): dynamic devices, whose headspaces are flushed by a forced flow (sweep air flow) passing through the device; and static devices (also called "static chambers"), the ones without the flush flow. The dynamic enclosure devices can be further divided into wind tunnels and flux hoods. Wind tunnels (e.g., Jiang et al., 1995; Sohn et al., 2005; Capelli et al., 2009b) are intended to promote a directional air flow, predominantly parallel to the liquid surface, and usually present a nominal air velocity. In contrast, flux hoods (e.g., Klenbusch, 1986; Blunden and Aneja, 2008), alternatively called "dynamic flux chambers", are normally designed as isolation-mixing chambers, with no representative value of air velocity.

The present study evaluates the flux hood whose design and basic operational conditions were presented by Klenbusch (1986) in a guide endorsed by the United States Environmental Protection Agency (US EPA). This device will be referred hereinafter as the "US EPA flux hood" (although the names "US EPA dynamic flux chamber" and "US EPA emission isolation chamber" are also frequently adopted in the literature). Originally proposed for the measurements of gaseous emissions from soils, posterior investigations extended the use of the US EPA flux hood for measurements of volatile emissions from liquid surfaces (Eklund, 1992). Initial evaluations of the method indicated satisfactory performance in terms of recovery rate (little losses within the equipment), precision (low variability among replicate measurement from a same individual flux hood) and repeatability (low variability among measurements from different individual flux hoods with identical design, placed side-by-side) (Kienbusch, 1986; Gholson et al., 1989, 1991; Eklund, 1992). Hudson and Ayoko (2008b) point out that the US EPA flux hood is suitable if standard, consistent and reproducible conditions are desired. As such, the US EPA flux hood has been widely adopted for measurement of volatile emissions, not only in the United States but also in many other countries (sometimes with modifications to methodology; for example, in Australia, the standard AS/NZS 4323.4:2009 adopts the same US EPA basic design, but includes an internal fan to enhance mixing).

Although it has been the subject of several studies (e.g., Gholson et al., 1991; Wang et al., 2001; Leyris et al., 2005; Sohn et al., 2005; Capelli et al., 2009b; Hudson and Ayoko, 2009; Hudson et al., 2009; Woodbury et al., 2011; Parker et al., 2013b; Guillot et al., 2014; Prata Jr. et al., 2016), there are still critical unsolved issues regarding the accuracy and applicability of the direct method, including the US EPA flux hood. A preliminary evidence that the method needs further investigation is the fact that significantly different emission rate measurements are produced if different enclosure devices are used in the same sources at the same time (for instance, pairs of devices are compared in Jiang and Kaye, 1996, Hudson and Ayoko, 2009, Hudson et al., 2009, and Parker et al., 2013b; Guillot et al., 2014, presents a compelling inter-comparison involving several devices). This is an indication that the internal aerodynamics and mass transfer conditions vary among the devices.

A major concern is that the conditions inside enclosure sampling devices do not resemble critical features of the atmospheric flow (and its interaction with the liquid surface) to which the water surface is exposed in the absence of the enclosure device (Gholson et al., 1989, 1991; Hudson and Ayoko, 2008a,b; Parker et al., 2013b), such as the levels of turbulence, boundary layer structure, surface currents and waves. Furthermore, due to the relatively low sweep air flow, some devices may present an artificial increase in the concentration of compounds (concentration build up) in their headspace, which can lead to a reduction of the emission rate during the experiment and an inappropriate measurement of the local emission rate (Hudson and Ayoko, 2008b). Local accumulation may also occur in case there is not enough mixing in the headspace (Gholson et al., 1989, 1991; Eklund, 1992; Woodbury et al., 2011). These aspects may compromise the accuracy of the emission rate measurements and the composition of odour samples produced by the application of direct sampling devices (Hudson and Ayoko, 2008a,b).

In an attempt to address some of the questions discussed in the previous paragraphs, Parker et al. (2013b) proposed a methodology for the standardisation of direct measurements of the emission rate of compounds in area sources. The approach consisted of quantifying the water evaporative fluxes from

116 containers placed inside the enclosure device (by weighting the container with water before and after a
117 certain time of operation) and using these fluxes to compare the emission rates of poorly volatile
118 compounds measured with different devices and scale up the results to the field situation. This is to be
119 done by means of water evaporative flux ratio correction factors, which are given by the ratio between
120 the evaporation rate measured with a container placed outside (close or on top of the emitting surface)
121 and the evaporation rate measured with an identical container inside the enclosure device. The method
122 is based on the fact that the volatilisation of poorly volatile compounds is controlled by transport
123 processes in the gas side of the gas-liquid interface (see theoretical discussion in section I of
124 Supplementary Material), which are the same processes responsible for the evaporation of water.
125 Nonetheless, the use of water evaporative flux ratio correction factors and other aspects of this approach
126 are subjected to some important restrictions, especially if the enclosure device presents concentration
127 build up in the headspace (discussed further in sub-section I.3 of Supplementary Material). On the other
128 hand, recently, Lucernoni et al. (2017) presented the scaling up of the emission rate measured with a
129 wind tunnel device for compounds with gas phase-controlled volatilisation, using a model for
130 representative values of wind speed that match the emission rate measured by the wind tunnel and allow
131 the recalculation for other values of wind speed. However, the resulting equations are specific for the
132 wind tunnel and the emission model adopted by those authors, and, therefore, cannot be directly extended
133 to the case of the flux hood.
134
135 Other recent studies have applied Computational Fluid Dynamics (CFD) in order to investigate different
136 enclosure devices (Eckley et al., 2010; Saha et al., 2011; Lin et al., 2012; Prata Jr. et al., 2014; Lucernoni
137 et al., 2016; Prata Jr. et al., 2016). The use of CFD enables a detailed representation of the fluid flow
138 pattern and the mass transfer inside the enclosure devices and, thus, provides extremely valuable
139 information for the understanding of their functioning and performance. However, as highlighted by
140 Prata Jr. et al. (2016), supporting experimental results are essential so as to validate and complement the

CFD simulations. Unfortunately, such experimental results are scarce in the literature, in special for flux hood-type devices.

The present study assessed the mass transfer inside the US EPA flux hood, with focus on the experimental determination of mass transfer coefficients in the microenvironment created by the flux hood and the effects of concentration build up in the hood`s headspace. The experiments comprised the evaporation of water and the volatilisation of different volatile organic compounds (VOCs), covering a range of behaviours regarding the dominance of the volatilisation process (volatilisation dominated by conditions in the gas phase, in the liquid phase and in both phases). Furthermore, the experimental results for the mass transfer of poorly volatile compounds (gas phase-dominated volatilisation) inside the US EPA flux hood were compared against an emission model for the passive surfaces in WWTPs. The evaluation of the US EPA flux hood as a method is of great relevance, given the widespread application of this device. Besides, the methodological and theoretical considerations presented here can be adopted for the assessment of other enclosure devices, in particular of flux-hood type.

2. METHODS

This section focuses on the experimental procedures to measure the rates of VOCs volatilisation and water evaporation inside the US EPA flux hood, which provided the basic information necessary for the determination of the overall, liquid-film and gas-film mass transfer coefficients, K_L, k_L and k_G, respectively.

Section I of the Supplementary Material presents a supporting theoretical analysis, treating the following topics:

- Definition of K_L, k_L and k_G and considerations about the mass transfer inside the flux hood, including the distinction among compounds with volatilisation dominated by the conditions in the liquid phase, in the gas phase and both phases.
- How to obtain K_L, k_L and k_G from the experimental results.
- A discussion about how concentration build up in the headspace can affect the mass transfer rates inside the flux hood.

The equations from Supplementary Material, when cited in this manuscript, are identified by "SM" before the equation number.

2.1. Flux hood design and operation

The flux hood used in this study, which can be seen in Figure 1a, was made of Plexiglas® and followed the design proposed by Klenbusch (1986), endorsed by the United States Environmental Protection Agency (US EPA). The standard design specifies a cylindrical body, with diameter of 40.6 cm and height of 17.8 cm, and a dome-shaped top whose highest part (at its central point) is 10.2 cm above the cylindrical body; our flux hood reproduces these dimensions with ± 1.3 cm difference. Also following the recommendations of Klenbusch (1986), there were four equidistantly-positioned holes on the top, one of which was an opening, with diameter 2.1 cm, for pressure equilibration and flow release. The other three had diameter 1.3 cm and were used to fit ¼" stainless steel bulkheads with the following purposes: one connected the sweep gas feed line to the internal inlet distribution tube; another connected the internal sampling probe to the outer sampling line; and the other was kept capped during most of the time of the runs, being used occasionally for checking the pressure differential between the interior of the hood and the external environment of the laboratory. The sweep gas distribution tube was made of stainless steel, ¼" OD, and fixed to the cylindrical body internal wall, at the height where the dome meets the body. It contained four equidistant inlet orifices, positioned horizontally (so as to produce

horizontal inlet jets), the one closest to the inlet bulkhead connection having diameter 2.0 mm, and the other three, diameter 2.4 mm. Figure SM1a (section II of Supplementary Material) illustrates the relative positioning of the inlet orifices and the holes at the top.

The sampling probe consisted of a 6" long tube, capped at the tip, perforated with two rows of holes, each row containing five holes with diameter 2.4 mm. The holes were separated 1" from each other along the tube length and positioned orthogonally in the radial direction. A Teflon® outlet line, ¼" OD, connected to the sampling probe via one of the bulkheads, conveyed the sampled flow to Nalophan® bags, which were filled using a "lung system" (Figure SM1b, section II of Supplementary Material) for the runs with sampling. The sweep air feed line, connecting the supplying gas bottle to the inlet distribution tube, was also Teflon® tubbing, ¼" OD.

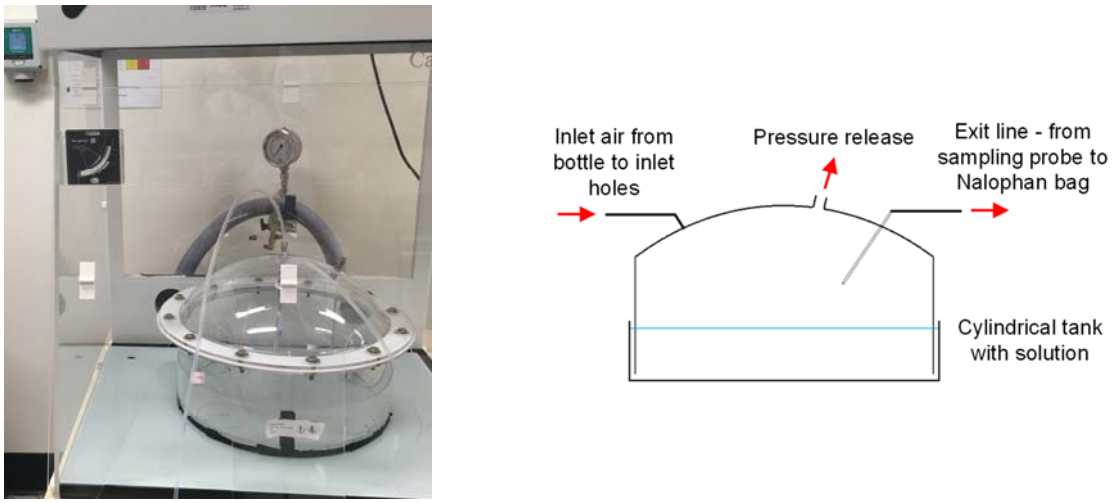

(a) (b)

Figure 1. Experimental setup: (a) US EPA flux hood, fit to the cylindrical tank; and (b) schematic representation of Figure 1a, identifying the inlet and outlet lines, and the pressure release.

The basic operation of the flux hood system was conducted according to the standard sampling procedure described by Kienbusch (1986), observing the additional recommendations of Eklund (1992) concerning

211 sampling on liquid surfaces. The sweep air feed was supplied by instrument-grade air bottles, with
212 maximum humidity content of 25 ppm (which can be approximated as completely dry air, for practical
213 purposes). The desired flow rates were adjusted by valve rotameters and checked using an electronic
214 flow rate meter (Mesa Labs – Defender 510). Two groups of experiments were carried out (sub-sections
215 2.2 and 2.3), which also present details of the operation of the flux hood system specific for each group.
216

217 **2.2. Volatilisation of compounds**

218

219 The flux hood sampling system was used to measure the rate of volatilisation from aqueous solutions of
220 compounds with different values of Henry's law coefficient (a broad compilation of Henry`s law
221 coefficients for various compounds of environmental interest is presented by Sander, 2015, which is
222 used in the present work), so as to cover the range of behaviours regarding the dominance of the
223 volatilisation process (section I of Supplementary Material): acetic acid, with volatilisation dominated
224 by conditions in the gas phase; chloroform and H_2S, with liquid phase-dominated volatilisation; and 1-
225 butanol, whose volatilisation, in the present experiment, was significantly dependent on both phases.
226 The compounds were assessed individually, in separate sets of experiments, for three nominal values of
227 sweep air flow rate, 2, 5 and 10 L min^{-1}; at each flow rate, runs were conducted in triplicate for each
228 VOC and in duplicate for H_2S. Additional triplicate runs were carried out for acetic acid and chloroform,
229 at a nominal flow rate of 5 L min^{-1}, using humidified sweep air (all the other runs used instrument-grade
230 dry air, which is the default condition).
231

232 VOC solutions were prepared by simply mixing a predefined volume of the pure compound (50 mL for
233 acetic acid, 2.5 mL for 1-butanol and 590 µL for chloroform) per litre of milliQ® water; the temperature
234 of the laboratory was recorded at the time of the mixing, making it possible to use the pure compounds`
235 density to obtain the value of their concentration in the solutions. The preparation of the H_2S solutions
236 followed a different procedure. An initial solution was produced, with sulfide (S^{2-}) concentration of 100

237 mg L^{-1}, by adding 0.375 g of solid sodium sulfide nonahydrate ($Na_2S.9H_2O$) in 500 mL of milliQ®
238 water; 10 mL of this solution were then diluted in 2 L of milliQ® water, achieving a nominal final
239 concentration of 0.5 mg L^{-1} S^{2-}. Just before the start of each run, the S^{2-} solution was acidified to a pH
240 lower than 4 using sulfuric acid, making all sulfide be in the non-dissociated form H_2S (Santos et al.,
241 2012).
242
243 The preparation of all the solutions took place shortly before the beginning of each experiment, so as to
244 avoid significant losses of the compounds. For each experimental run, 1.7 L of the solution was
245 transferred to a cylindrical tank made of Plexiglas®, with diameter 41.0 cm and height 8.5 cm; the depth
246 of the liquid in the tank was approximately 1.3 cm. The flux hood was then fit to the cylindrical tank
247 (Figure 1a,b), and the sampling and sweep air flow started immediately. The sweep air flow rate was
248 then finely-adjusted to the desired value with the help of the in-line electronic flow meter. The flow rate
249 in the sampling line was 200 mL min^{-1} for all the runs, guaranteed by previous calibration of the lung
250 system. After the adjustment of the sweep air flow rate, the so-called stabilisation time started, following
251 the recommendation of Klenbusch (1986) that valid samples should be collected only after waiting some
252 time (minimum of four residence times) so the internal air flow and mass transfer achieve a stabilised
253 condition. The stabilisation times adopted in the present study were: 30 min for the flow rates of 5 L
254 min^{-1} and 10 L min^{-1}, and 60 min for the flow of 2 L min^{-1}. After the stabilisation time, the bag in the
255 lung system was replaced, starting then the valid sampling time, which varied between 20 to 30 min for
256 each run; the sample collected during the stabilisation time was discarded.
257
258 The internal pressure in the flux hood was equilibrated with the pressure in the laboratory environment,
259 which was systematically monitored using a differential manometer. The temperatures of the liquid in
260 the tank and of the laboratory environment were measured at the beginning and the end of the sampling
261 time. The laboratory temperature was 19.0 ± 1.0 ˚C, whilst the temperature of the liquid ranging from
262 17.9 to 21.5 ˚C among the runs, with average 20.0 ˚C. The sweep air flow rate was also verified at the

263 end of the sampling time, the value being recorded (together with the initially adjusted value) to be used
264 in the subsequent calculations. Since part of the H_2S was expected to escape during the acidification step
265 (thus the nominal concentration when the solution was prepared would significantly differ from the
266 actual concentration in the experiment), for the experiments with H_2S, samples of the solution in the
267 tank were collected at the beginning and end of the valid sampling time, by inserting a pipette through
268 the pressure-equilibration opening at the top of the flux hood. The sulfide concentration in these liquid
269 samples (dissolved S^{-2}) was determined via the methylene blue method coupled with spectrophotometry
270 (equivalent to APHA, 2005, method 4500-S^{2-} D), using a HACH spectrophotometer (HACH – DR1900)
271 and analysis kit.
272
273 For all compounds, the gas samples collected in the Nalophan® bags during the valid sampling time
274 were analysed within maximum one hour of the time of sampling, thereby preventing any possible
275 significant losses of the compounds via diffusion through the bags. The concentration of H_2S was
276 measured using a H_2S analyser (Jerome – 631-X, Arizona Instrument, USA). The concentrations of the
277 VOCs were quantified by gas-chromatography (GC) – 7890A (Agilent Technologies, USA), equipped
278 with a micro-cell electron capture detector (μECD) and a flame ionisation detector (FID), employing a
279 capillary column Agilent Plot Q, 30 m × 535 μm × 40 μm, with He as carrier gas. The gas samples were
280 manually injected using a gas-tight syringe. Acetic acid and 1-butanol were detected by the FID, with
281 detector temperature 250 ˚C and N_2 make-up flow of 25 mL min^{-1}; injector temperature was 250 ˚C,
282 operating in "splitless" mode, and the carrier gas flow in the column was 9 mL min^{-1}. Chloroform was
283 analysed by the μECD, with detector temperature 150 ˚C and N_2 make-up flow of 30 mL min^{-1}; injector
284 temperature was 250 ˚C, operating in "split" mode (split ration 100:1), septum purge flow of 3 mL min^{-1},
285 and carrier gas flow of 3.5 mL min^{-1} in the column. The oven temperature programme was different
286 for each compound: for acetic acid, an initial temperature of 180 ˚C was hold for 1 min, then increased
287 at a rate of 100 ˚C min^{-1} to 220 ˚C, then maintained for 7 min; for 1-butanol, the initial temperature was

288 also 180 ˚C, hold for 1 min, then increased at a rate of 20 ˚C min^{-1} to 200 ˚C, maintained for 0.7 min,
289 and increasing again, at a rate of 100 ˚C min^{-1} to a final temperature of 210 ˚C, maintained for 3 min;
290 for chloroform, the initial temperature was 150 ˚C, hold for 0.5 min, then increased at a rate of 30 ˚C
291 min^{-1} to a final temperature of 250 ˚C, maintained for 1 min. Calibration curves for each compound were
292 established using gas samples at five known concentrations, produced by evaporating different amounts
293 of pure standard solutions of the compounds into Nalophan® bags flushed with fixed volumes of sweep
294 air (preparation method adapted from Wang et al., 2015).
295
296 Following the standard procedure for the use of the US EPA flux hood (Klenbusch, 1986), the measured
297 gas-phase concentrations C_m (kg m^{-3}) were used in Equation (1) to estimate the volatilisation rate of the
298 compounds J (kg s^{-1} m^{-2}), being Q the sweep air flow rate (m^3 s^{-1}) and A the area (m^2) of the surface
299 enclosed by the hood ("footprint area"). Implicit in Equation (1) is the idea that the concentration in the
300 samples collected via the sampling probe represents the mean concentration in the total outlet flow
301 (which comprises the small fraction that is sampled plus the majority of the flow that is released by the
302 pressure equilibration hole at the top of the flux hood). This, in turn, would be guaranteed by a
303 completely-mixed bulk gas phase inside the hood. Preliminary CFD simulations by Prata Jr. et al. (2016)
304 indicated differences between the sampled flow and the total outlet flow of order 7%, for flux hood
305 configuration and operational conditions slightly different from the present study. Differences for the
306 present case can be expected to be of the same order, thus the volatilisation rates calculated using
307 Equation (1) can be assumed satisfactorily accurate in the context of the mass transfer experiments
308 treated herein.
309

$$J = \frac{Q C_m}{A} \quad (1)$$

310

311 Additional tests were conducted with acetic acid and chloroform, at a nominal flow rate of 5 L min^{-1}, in
312 order to assess the influence of high humidity in the sweep air flow on the volatilisation rate of these
313 compounds. The procedure for these tests were the same as previously described, except that the sweep
314 air flow was passed through a bubbling column before entering the flux hood inlet distribution line. The
315 bubbling column was filled with milliQ® water, 30 cm deep, and had a relatively large diameter, which
316 avoided significant changes in the depth of the water column during the course of a run, therefore
317 avoiding significant changes in the head losses along the feed line, consequently stabilising the flow
318 rate. The relative humidity in the sweep air flow exiting the bubble column was approximately 90%,
319 measured by an electronic relative humidity sensor before and after each run. Volatilisation rates were
320 also calculated using Equation (1).
321
322 **2.3. Water evaporation**
323
324 Water evaporation experiments were performed aiming to adapt and assess the use of the water
325 evaporative rate method (Parker et al., 2013b) applied to the US EPA flux hood to characterise the
326 overall mass transfer inside the flux hood, under different operational conditions. Because the mass
327 transfer conditions are not uniform along the surface enclosed by the hood (Parker et al., 2013b; Prata
328 Jr. et al., 2016), it is important that the evaporation source corresponds to the whole footprint area.
329 Following this premise, the Plexiglas® cylindrical tank (sub-section 2.2) was employed as the
330 evaporation pan for the water evaporation experiments. The evaporation rates were evaluated for nine
331 different set of conditions: three nominal values of sweep air flow rate, 2, 5 and 10 L min^{-1}, times three
332 nominal humidity contents in the sweep air, relative humidity of 0% (dry air), 45% and 90%. For each
333 set of conditions, triplicate runs were conducted.
334
335 The humidity contents in the sweep air were achieved using the bubbling column system (sub-section
336 2.2). For the relative humidity of 90%, all the feed air flow was passed through the bubbling column.

337 For the relative humidity of 45%, the feed air flow was split in two parallel lines, with only one of them
338 (i.e., approximately half of the total flow) passing through the bubbling column; the two lines joined
339 again by means of a T-joint and the resulting single line connected to the inlet distribution system of the
340 flux hood (Figure SM2, section II of Supplementary Material). In each run, the actual humidity content
341 in the sweep air feed line differed slightly from the nominal values, depending mainly on temperature
342 and flow rate, and was measured by an electronic relative humidity sensor before and after the run.
343
344 Before the start of a run, the tank was filled with 1.7 L of milliQ® water, and the precise mass of the
345 filled tank was recorded using a laboratory scale with precision of 0.1 g. After weighting the tank, the
346 flux hood was fit to it, and the small gaps between the hood and the tank walls sealed with Parafilm®
347 (fixed with adhesive tape) to avoid evaporation losses through the gaps; this was necessary, since it was
348 verified that the undesired collateral evaporation could affect significantly the measured evaporation
349 rate. The feed gas line was then connected to the hood, starting the experimental run, and the sweep air
350 flow rate was finely-adjusted to the desired value with the help of the in-line electronic flow meter; the
351 value of the flow rate was also checked at the end of each run. There was no sampling in the evaporation
352 experiments, and the sampling outlet line was kept sealed and inactive. The flux hood operated under
353 isobaric condition. The laboratory temperature was 19.0 ± 1.0 ˚C, and the temperature of the water
354 ranged from 17.2 to 19.0 ˚C among the runs, with average 18.3 ˚C.
355
356 For the experiments with dry sweep air, the run time was 2 h, for which the change in the mass of the
357 water in the tank was well above the precision of the scale whereas the water level in the tank was not
358 significantly affected; it was also verified that the measured evaporation rates did not change if longer
359 runs were performed. The duration of the runs for the experiments with humid sweep air was longer, so
360 as to allow for an amount of evaporation that would promote a detectable change in the mass of the water
361 in the tank. At the end of the run, the feed gas line was disconnected, the Parafilm® seal removed, and
362 the mass of the tank with water was again weighted on the scale. The evaporation rates J_w (kg s^{-1} m^{-2})

were calculated via Equation (2), where m_0 and m_f are the initial and final mass (kg) of the filled tank, and Δt is the duration of the run (s). If desired, the evaporation rate can be straightforward converted in mm d^{-1} by using the water density (which is function of the water temperature) and converting units.

$$J_w = \frac{(m_0 - m_f)}{A\,\Delta t} \quad (2)$$

3. RESULTS AND DISCUSSION

3.1. Volatilisation and evaporation rates under different sweep air flow rates

Figure 2 presents the variation of the volatilisation rates J of the VOCs and H_2S with the sweep air flow rate (Q). As a trend, the emission rates of all compounds increased with the flow rate. The behaviour of the measured emission rate of acetic acid and 1-butanol, for which the volatilisation is controlled by conditions in the gas phase and in both phases, respectively, is similar to the reported by Rhoades et al. (2005) for the flux of ammonia, whose volatilisation is controlled by both phases, measured with the US EPA flux hood in a lagoon. The increase in the volatilisation rates of chloroform and H_2S, both liquid phase-controlled, contrasts with the results of Gholson et al. (1989), who found that the emission rates of 1,1,1-trichloroetane (also liquid phase-controlled) measured with the US EPA flux hood did not present any clear pattern of variation with the flow rate. This difference may be attributed to the fact that, in the present study, the only dynamical forcing in the liquid phase was the friction produced by the sweep air flow on the water surface whereas in the experiments of Gholson et al. (1989) the flux hood was placed inside an apparatus that simulates a wind blowing over the surface of a small tank, which generated surface currents. It is possible that the interaction of these surface currents with the edge of the flux hood was the main source of turbulence and the main driver for mass transfer in their

387 case, surpassing the effects of any changes in the relatively weak friction of the sweep air inside the
388 hood.
389
390 The variation of the volatilisation rates with the sweep air flow, observed in Figure 2, reflects the
391 combined effect of the changes in the mass transfer coefficients and in the accumulation of compounds
392 in the hood`s headspace. The experimental mass transfer coefficients are examined in more detail in
393 sub-section 3.2. Being C_L and C_G the concentration of the compound (kg m^{-3}) in the bulk of the liquid
394 and the gas phases, respectively, and K_H the non-dimensional Henry`s law coefficient ($K_H = C_G/C_L$ for
395 the equilibrium situation), the importance of accumulation can be preliminarily assessed by examining
396 the relative magnitude of C_G/K_H compared to C_L (Equation (SM3a)). For a well-mixed headspace, as in
397 the present case, C_G can be approximated by the concentration C_m measured for the sample collected in
398 the Nalophan® bags. For acetic acid, C_G/K_H was between 46% to 81% of the corresponding C_L, and for
399 1-butanol, C_G/K_H ranged from 54% to 92% of C_L. This confirms that concentration build up inside the
400 flux hood is significant for the mass transfer of compounds whose volatilisation is affected by the gas
401 phase (gas phase or both phase-controlled volatilisation). Conversely, for chloroform and H_2S, C_G/K_H
402 was less than 1% of C_L in all the experiments, indicating that the accumulation in the hood`s headspace
403 was not relevant for the compounds with liquid phase-controlled volatilisation, consistent with the
404 theoretical considerations made previously (sub-section I.3 of Supplementary Material).
405
406

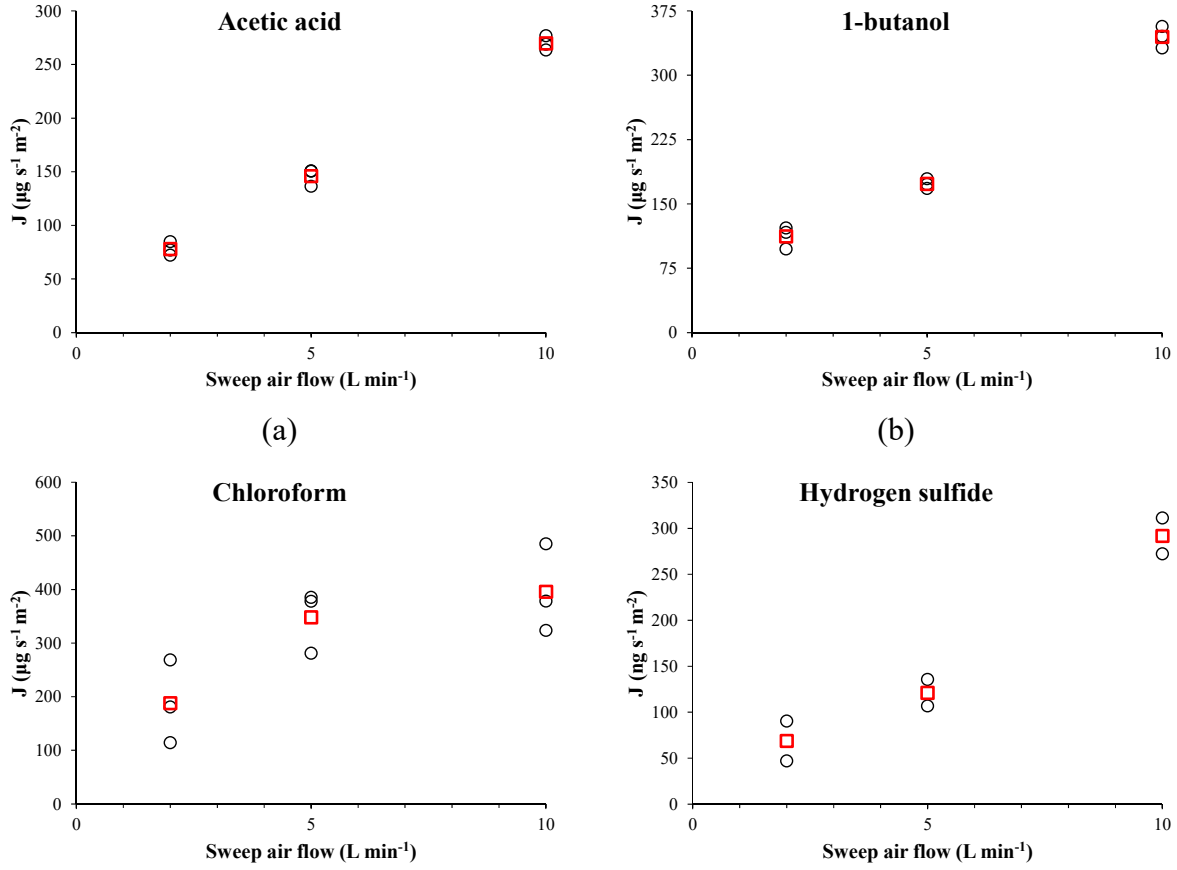

407 Figure 2. Volatilisation rates of VOCs and hydrogen sulfide measured by the flux hood operating with
408 different sweep air flow rates. Black circles represent results of individual experimental runs, and the
409 red squares indicate the average volatilisation rate at each nominal flow rate.

410

411 Figure 3a shows how the water evaporation rate inside the flux hood varies with the sweep air flow rate,
412 for different values of humidity content in the inlet air. Similarly to the volatilisation rate of compounds,
413 J_w generally increases with Q. As expected, at a given sweep air flow rate, J_w is smaller for higher
414 humidity content in the inlet air. For dry inlet air (RH = 0%), the behaviour (and, to a certain degree, the
415 values) of J_w is similar to the results of Parker et al. (2013b) for an evaporation source covering the
416 whole footprint of the flux hood, which is an evidence of the relatively good repeatability of the US EPA
417 flux hood, an attribute classically associated with this device.

418

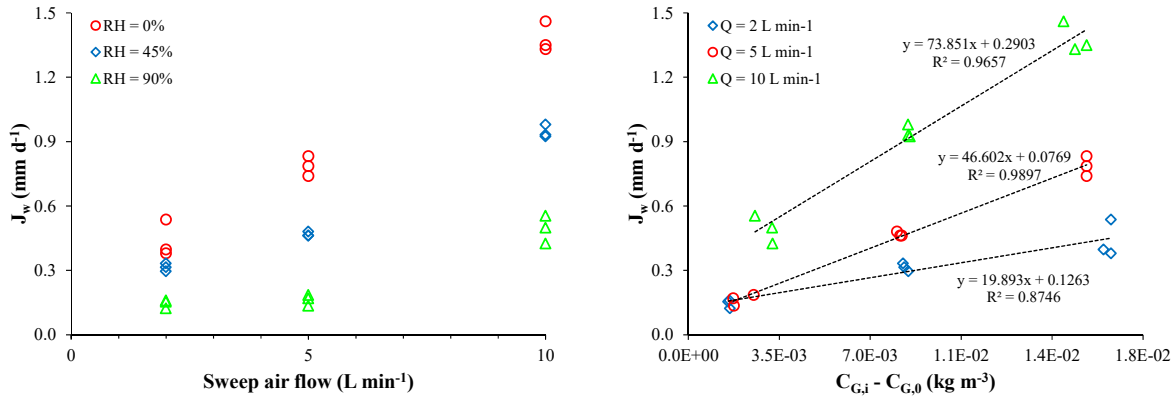

(a) (b)

Figure 3. Variation of the water evaporation rate J_w with: (a) the sweep air flow rate, three nominal inlet relative humidity values (legend in (a)); and (b) the difference between $C_{G,i}$ and $C_{G,0}$, for the three nominal sweep air flow rates (legend in (b)).

In Figure 3b, it can be observed that, for a given Q, the water evaporation rate J_w increases as the difference between the concentration (kg m^{-3}) of water vapour at the gas side of the gas-liquid interface ($C_{G,i}$) and in the inlet air ($C_{G,0}$) becomes larger. The seemingly linear fashion with which J_w varies as a function of the difference $C_{G,i} - C_{G,0}$ is consistent with Equation (SM6), except for the existence of a non-zero, positive intercept in the experimental lines (in contrast, according to Equation (SM6), J_w should be strictly proportional to the difference $C_{G,i} - C_{G,0}$). Possibly, the main reason for this deviation is the difficulty of accurately determining the temperature at the water surface, which is necessary to estimate $C_{G,i}$ (Parker et al., 2013b, also points out the same difficulty); in the present experiments, the bulk temperature of the water in the Plexiglas® tank is used. An additional factor that may have contributed is the uncertainty in the measurement of the relative humidity in the inlet air, which is converted into $C_{G,0}$. On the other hand, although the experimental procedure was designed in order to avoid losses of water by collateral evaporation, the possibility of minor losses contributing to the positive offset identified in Figure 3b cannot be totally discarded.

437 It is worth mentioning that, with dry inlet air, the average volatilisation rates J are positively correlated
438 with the corresponding water evaporation rates J_w; the plots of J against J_w for the four VOCs are
439 presented in Figure SM3 (section II of Supplementary Material). For acetic acid (gas phase-controlled
440 volatilisation), the variation of J with J_w appears to be almost linear (but not exactly proportional),
441 although more values are necessary to verify if linearity actually holds. As discussed in sub-section I.3
442 (Supplementary Material), the water evaporation method (Parker et al., 2013b) is not necessarily
443 applicable to inter-convert between volatilisation rates measured with the US EPA flux hood under
444 different operational conditions. However, the almost-linearity observed for acetic acid (Figure SM3a)
445 suggests that the water evaporation method may be used in order to approximate relative changes in the
446 magnitude of the volatilisation rate of gas phase-dominated compounds due to changes in the sweep air
447 flow rate. It can also be useful to qualitatively compare the overall mass transfer conditions in the
448 headspace of the US EPA flux hood under different operational conditions.
449
450 **3.2. Mass transfer coefficients inside the flux hood**
451
452 Table 1 presents the average, minimum and maximum of the experimental values of the overall mass
453 transfer coefficient K_L for all compounds, the liquid-film mass transfer coefficient k_L for chloroform and
454 H_2S (liquid phase-controlled volatilisation) and the gas-film mass transfer coefficient k_G for acetic acid
455 (gas phase-controlled volatilisation), obtained by the procedure explained in sub-section I.2
456 (Supplementary Material). The variation of the experimental k_G and k_L with Q is illustrated in Figure
457 4a-c. The mass transfer coefficients generally increased with the sweep air flow rate, reflecting the
458 enhancement of the near-interface turbulence that is expected to occur as Q rises. The only case that
459 appears not to conform to this overall trend is the K_L for 1-butanol at Q = 2 L min^{-1}. This is probably due
460 to the difficulty of determining the temperature at the water surface, as mentioned before, and the
461 uncertainty in the value of the Henry`s law coefficient K_H (also noticing that this case presented a
462 particularly large difference between minimum and maximum values).

463

464 **Table 1.** Experimental mass transfer coefficients.

Compound	**Coefficient**								
				K_L **(10^{-9} m s^{-1})**					
	Q = 2 L min^{-1}			**Q = 5 L min^{-1}**			**Q = 10 L min^{-1}**		
	average	min	max	average	min	max	average	min	max
Acetic acid	7.1	5.5	9.1	7.4	6.4	7.9	13.5	12.3	15.3
1-butanol	470.6	183.5	794.0	200.0	185.4	224.7	451.2	447.1	453.3
Chloroform	242.7	154.0	337.3	431.6	364.1	469.5	507.1	434.3	600.4
Hydrogen sulfide	249.2	198.4	300.0	363.4	352.9	374.0	1076.9	825.2	1328.5
				k_L **(10^{-7} m s^{-1})**					
	Q = 2 L min^{-1}			**Q = 5 L min^{-1}**			**Q = 10 L min^{-1}**		
	average	min	max	average	min	max	average	min	max
Chloroform	2.427	1.540	3.373	4.316	3.641	4.695	5.071	4.343	6.004
Hydrogen sulfide	2.492	1.984	3.000	3.634	3.529	3.740	10.769	8.252	13.285
				k_G **(10^{-3} m s^{-1})**					
	Q = 2 L min^{-1}			**Q = 5 L min^{-1}**			**Q = 10 L min^{-1}**		
	average	min	max	average	min	max	average	min	max
Acetic acid	1.001	0.802	1.253	1.059	0.945	1.122	2.103	1.808	2.454

465

466

467

468

469

470

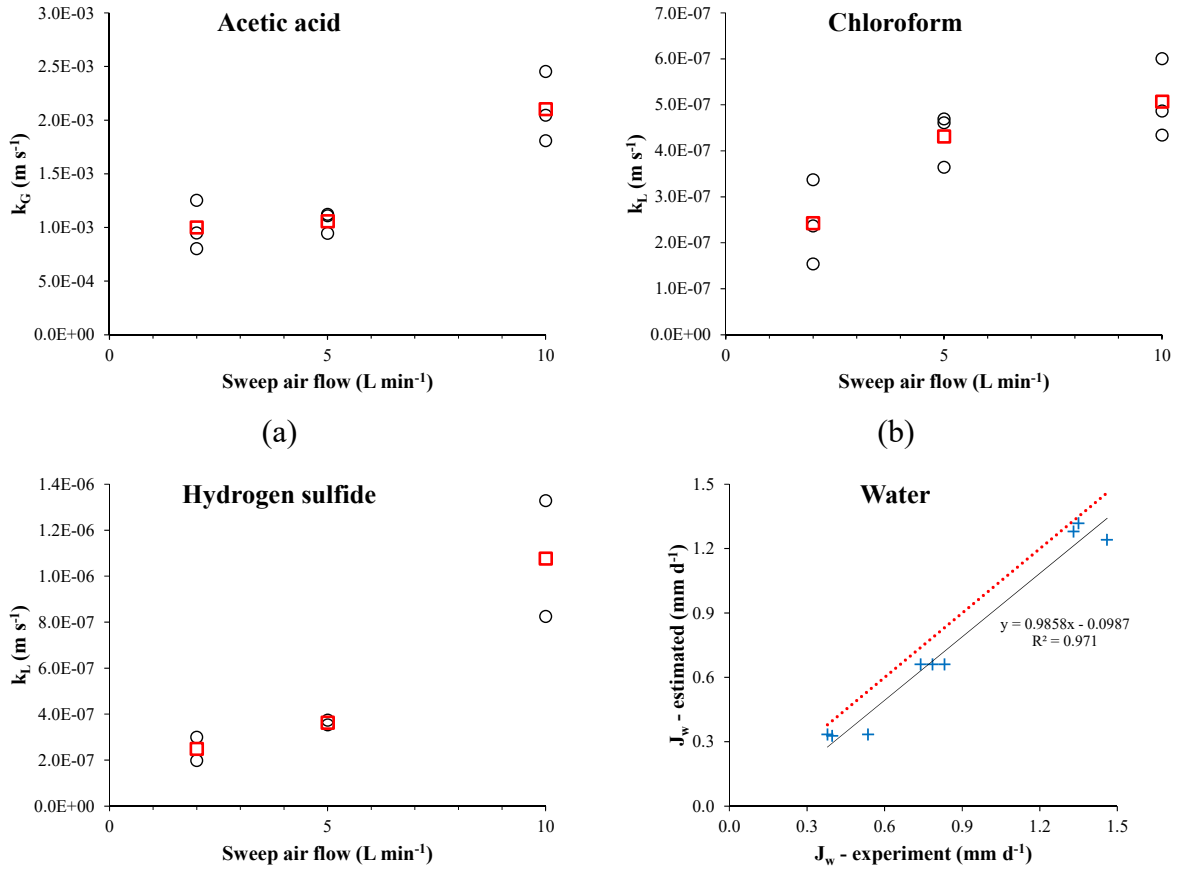

471 Figure 4. Variations with the sweep air flow rate of the experimental (a) gas-film mass transfer
472 coefficient k_G for acetic acid and the liquid-film mass transfer coefficients k_L for (b) chloroform and (c)
473 H_2S inside the US EPA flux hood; and (d) comparison between the experimental water evaporation rate
474 J_w and the J_w estimated by applying Equation (SM6) with k_G for water calculated based on k_G for acetic
475 acid, using Equation (SM4a). In (a)-(c), the black circles represent results of individual experimental
476 runs, and the red squares indicate the respective average at each nominal flow rate; in (d), the red dotted
477 line is the 1:1 line, and the black line is the linear fit to the results (equation shown in the figure).
478
479 Despite being feasible in theory (sub-section I.2 of Supplementary Material), the calculation of k_G for
480 water vapour directly from the experimental evaporation rates J_w was not possible in the present
481 circumstances, producing unreasonable values of k_G (some of which negative). This is a result of two
482 factors: again, the imprecision of the measurements of the temperature at the water surface, which, as a
483 consequence, makes the estimate of $C_{G,i}$ not precise; and the apparent offset verified in J_w (sub-section

484 3.1) this would lead to an overestimation of C_G, as per Equation (SM5). For water vapour and other gas
485 phase-controlled compounds, the accumulation in the headspace significantly interferes with the
486 emission rates, as identified before (sub-section 3.1), since the differences between $C_{G,i}$ and C_G (or,
487 alternatively, between C_L and C_G/K_H) are relatively small. This same fact may also affect the calculation
488 of K_L (or k_G, for water vapour) for such compounds by solving Equations (SM3a) (or (SM1)), given that
489 the difference $C_L - C_G/K_H$ (or $C_{G,i} - C_G$) will be very sensitive to the uncertainties in the values of C_G
490 and K_H (or $C_{G,i}$ and J_w, for water vapour), which is observed in some of the cases reported herein (K_L
491 for 1-butanol at Q = 2 L min^{-1} and k_G for water vapour).
492
493 This highlights some of the challenges inherent to the experimental determination of mass transfer
494 coefficients for gas phase-controlled compounds in a mixed-headspace device such as the US EPA flux
495 hood, if the a ratio A/Q is not large enough to avoid significant accumulation in the gas phase. In special,
496 the necessity of appropriate values of K_H and high-precision measurements of the temperature at the
497 water surface is clear, both of which are not always straightforward available. The difficulty of having
498 accurate temperature values at the water surface, preventing the satisfactory calculation of k_G based on
499 the water evaporation rates, was already noted by Parker et al. (2013b) when the water evaporation
500 method was originally devised. The effects of accumulation in the headspace can be minimised by
501 adopting water tanks with smaller surface area; for instance, Parker et al., 2013b, propose the use of Petri
502 dishes as evaporation sources. However, this practice is not suitable for the study of the US EPA flux
503 hood because the mass transfer conditions are not uniform along the hood`s footprint, as evidenced by
504 Parker et al. (2013b) and Prata Jr. et al. (2016). Thus, for the correct assessment of the mass transfer
505 inside the US EPA flux hood, the simulated emission source has to encompass the whole footprint of
506 the flux hood.
507

508 In order to verify the accuracy of the k_G values for acetic acid, Equation (SM4a) was applied to estimate
509 k_G for water vapour based on the average experimental k_G of acetic acid at the three sweep air flow
510 rates. The estimated water vapour`s k_G is then used in Equation (SM6) to obtain estimates of J_w
511 (considering dry inlet air), which are compared against the experimental J_w in Figure 4d. As seen in this
512 figure, the estimated k_G produced J_w values in relatively close agreement with the experimental ones
513 (average relative error of -15.1%) and also correctly represented the pattern of variation of J_w with Q,
514 indicated by the good linear fit with slope close to 1 (black line and equation in Figure 4d). The slight
515 underestimation in J_w are consistent with the apparent offset reported (sub-section 3.1). These results
516 validate the experimental values of k_G for acetic acid and show that they can be used to characterise the
517 magnitude of mass transfer in the gas phase inside the US EPA flux hood, under the studied operational
518 conditions. Furthermore, they support the use of Equation (SM4a) to estimate k_G for other compounds
519 based on the experimental k_G for acetic acid.
520
521 Table 2 presents experimental values of k_G reported by different authors that used wind tunnel-type
522 devices. Since the compounds used in the studies were not the same, for better comparison, Table 2 also
523 includes the expected k_G for each compound in the US EPA flux hood operating with sweep air flow of
524 5 L min^{-1} (which is the typical operation), estimated using the average k_G for acetic acid in the flux hood
525 found in the present experiments (for Q = 5 L min^{-1}) and Equation (SM4a). It is interesting to notice that,
526 except for the highest nominal velocity tested by Parker et al. (2008), k_G in the flux hood is of the same
527 order as the respective k_G observed in the wind tunnels, sometimes higher. However, due to the
528 concentration build-up in the flux hood`s headspace (which normally in inexistent or very small in wind
529 tunnels), the emission rates measured by the US EPA flux hood may be significantly lower than the
530 emission rates measured by wind tunnels. An assessment of this effect is also shown in Table 2, which
531 contains the ratio between the volatilisation rate that can be expected to happen in the wind tunnel (which
532 can be estimated by Equation (SM1), using the wind tunnel`s k_G and considering $C_G \approx 0$) and the

533 volatilisation rate that would take place inside the flux hood (calculated by Equation (SM7b), using the
534 estimated k_G for the compound in the flux hood), considering the same concentration $C_{G,i}$ at the gas-
535 liquid interface. The ratios varied from 1.69 to 19.23, and depend on the compound, the type of wind
536 tunnel and its operational conditions.

537

538 **Table 2.** Mass transfer coefficients reported in the literature for wind tunnel devices and comparison
539 with the US EPA flux hood (operating with sweep air flow of 5 L min^{-1}).

Reference	Compound	Nominal conditions for the wind tunnel	k_G (m s^{-1})	k_G (m s^{-1}) in the flux hood[a]	Ratio for J in wind tunnel/flux hood[b]
Bliss et al. (1995)	Ammonia	Nominal velocity 0.33 m s^{-1}	1.788×10^{-3}	1.726×10^{-3}	3.64
Parker et al. (2008)	Water	Nominal velocity 0.003 m s^{-1}	9.167×10^{-4}	2.601×10^{-3}	1.69
		Nominal velocity 0.133 m s^{-1}	1.045×10^{-2}	2.601×10^{-3}	19.23
Capelli et al. (2009b)	1-butanol	Nominal velocity 0.138 m s^{-1}	7.754×10^{-4}	1.233×10^{-3}	1.76
		Nominal velocity 0.6 m s^{-1}	9.892×10^{-4}	1.233×10^{-3}	2.24

540 [a]k_G for the same compound, calculated using the experimental k_G for acetic acid in the flux hood found in this research and
541 Equation (SM4a).
542 [b]Ratio between the volatilisation rate that would be measured by the wind tunnel (calculated by Equation (SM1), using the
543 wind tunnel`s k_G and considering $C_G \approx 0$) and the respective rate that would be measured by the US EPA flux hood (calculated
544 by Equation (SM7b), using the estimated k_G for the compound in the flux hood), considering the same $C_{G,i}$.
545

546 Regarding the liquid-film mass transfer coefficient k_L, the results for chloroform and H_2S showed that
547 k_L increased with Q, suggesting that the small motions induced in the liquid by the friction of the sweep
548 air flow above (which is expected to be more intense for larger Q) were the main drivers of mass transfer
549 in the liquid side, as anticipated in sub-section 3.1. Nevertheless, if surface currents are present, the
550 interaction of these currents with the edge of the flux hood will likely dominate the mass transfer in the
551 liquid, as also discussed before. Comparing Figures 6b and 6c, it can be seen that the proportional
552 changes in k_L with Q did not follow the same pattern for chloroform and H_2S, which can be attributed
553 to unavoidable small losses of these highly volatile compounds that may have occurred during the
554 preparation of the solutions and when the solutions were transferred to the tank. Because such losses
555 would happen in a rather random way, this is consistent with the relatively large large difference between

556 minimum and maximum values of k_L observed for these compounds, especially for Q = 10 L min^{-1}.
557 However, the results for both chloroform and H_2S agree in terms of the order of magnitude of k_L in the
558 micro environment under the sole influence of the US EPA flux hood, and this can be used for the
559 analysis in sub-section 3.3.
560
561 Tests were also performed with acetic acid and chloroform, with Q = 5 L min^{-1}, aiming to assess the
562 sensitivity of, respectively, k_G and k_L to changes of humidity in the sweep air flow. With relative
563 humidity of approximately 90% in the inlet air, the average k_G for acetic acid inside the flux hood was
564 7.500×10^{-4} m s^{-1} (minimum 6.050×10^{-4} m s^{-1}, maximum 9.470×10^{-4} m s^{-1}), and the average k_L for
565 chloroform was 4.372×10^{-7} m s^{-1} (minimum 4.199×10^{-7} m s^{-1}, maximum 4.628×10^{-7} m s^{-1}). Considering
566 a level of significance of 10%, an analysis of variance (ANOVA) indicates that k_G is affected by the
567 humidity in the inlet air (p-value = 0.058), whilst k_L is not (p-value = 0.885). It can be hypothesised that
568 one or both of the following mechanisms account for the slight difference in k_G between the cases with
569 dry and humid inlet air. (i) Being a poorly volatile compound, part of the volatilised acetic acid in the
570 headspace of the chamber may have been absorbed in the little droplets of water that condensed on the
571 flux hood`s walls when humid inlet air was employed, leading to an apparent reduction of k_G. (ii) It may
572 be possible that additional turbulence generated by buoyancy due to the difference in density between
573 the lighter, saturated air close to the water surface and the heavier, dry inlet air contribute to the near-
574 interface mass transfer (i.e., to k_G); with humid inlet air, this buoyancy would be greatly reduced, making
575 k_G smaller. It is important to highlight that the volatilisation rates of acetic acid are relatively less
576 sensitive to the change in the sweep air humidity, buffered by the effect of accumulation in the
577 headspace: while the average k_G decreased by 29%, the average J was only 14% smaller.
578
579 **3.3. Relating measurements obtained with the flux hood and field emission rates**
580

581 By knowing the values of the mass transfer coefficients in the interior of the flux hood, it is possible to
582 estimate the bias in the measured emission rate, compared to the values that could be expected in the
583 field in the absence of the sampling device, especially for compounds with volatilisation controlled by
584 conditions in the gas phase. In the present analysis, the k_G calculated by the volatilisation model
585 proposed by Gostelow et al. (2001a) for passive liquid surfaces is adopted as a proxy for the k_G values
586 in the field. The friction velocity, which is one of the input variables for the model, is estimated based
587 on the wind speed at 10 m height (U_{10}) by applying the correlation of Smith (1980). Figure 5a shows k_G
588 for acetic acid estimated by the model for U_{10} varying from 0 to 10 m s^{-1}. For comparison, the respective
589 average k_G inside the US EPA flux hood obtained in our experiments for the sweep air flow rates of 2,
590 5 and 10 L min^{-1} are also indicated in Figure 5. It is clear that the k_G in the flux hood represent conditions
591 of low wind speeds; more specifically, for the flow rates of 2, 5 and 10 L min^{-1}, the k_G for acetic acid
592 equal the model estimates for U_{10} = 1.18, 1.25 and 2.36 m s^{-1}, respectively. Figure 5b presents the ratios
593 between the k_G calculated by the model and the experimental k_G in the flux hood, for acetic acid at
594 various U_{10}.
595
596 Nevertheless, because of the build-up of concentration in the headspace of the hood (an effect that does
597 not occur for open surfaces in the field), the volatilisation rates inside the flux hood will be lower than
598 the corresponding volatilisation rates in the field, for the same k_G. To illustrate this, Figure 5c shows the
599 emission rates J of acetic acid predicted by applying Gostelow et al.`s (2001a) model, considering the
600 concentration in the liquid C_L = 10 g L^{-1} and U_{10} ranging from 0 to 10 m s^{-1}. For the same C_L, the
601 volatilisation rates inside the flux hood were estimated by using the experimental k_G together with
602 Equation (SM7b) (considering $C_{G,i} \approx C_L K_H$, which is valid for poorly volatile compounds such as acetic
603 acid) and are indicated by the traced lines in Figure 5c. Figure 5d presents the ratios between the J
604 calculated by the model for the field and the expected J in the flux hood, for the same concentration C_L
605 of acetic acid at various U_{10}. It is interesting to notice that the emission rates of acetic acid that would

606 be observed in the flux hood operating with Q = 2, 5 and 10 L min^{-1} are equivalent to the field J at U_{10}
607 = 0.27, 0.51 and 0.99 m s^{-1}, respectively (the estimates for J and the respective field-to-flux hood ratio
608 in the low wind speed range is shown in detail in Figures 5e and f). Such equivalencies for J will change
609 depending on the compound (different k_G).
610

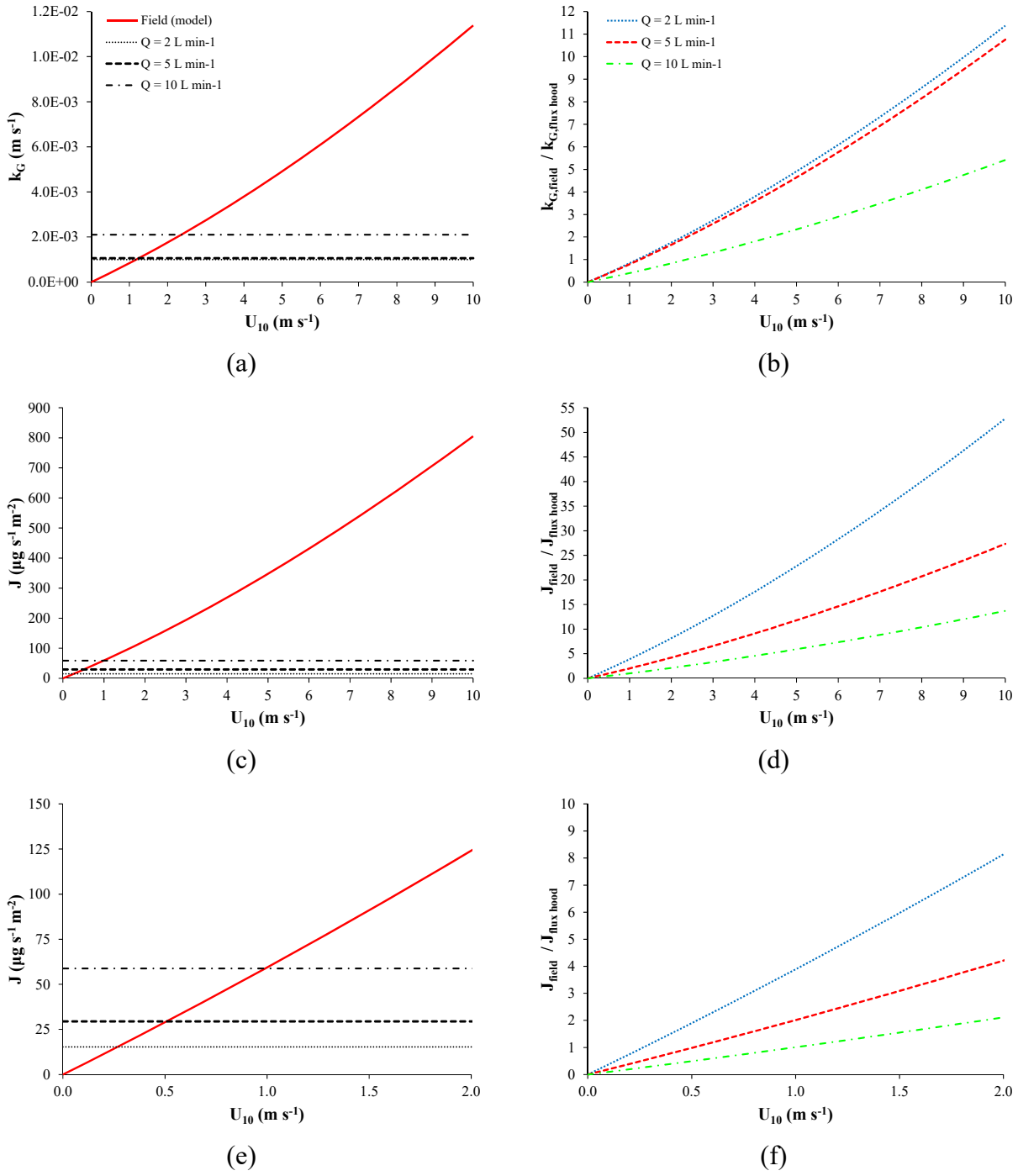

611 Figure 5. Comparison between the mass transfer of acetic acid inside the US EPA flux hood and a
612 modelled field situation (model of Gostelow et al., 2001a), for wind speeds at 10 m (U_{10}) varying from
613 0 to 10 m s^{-1}, showing the values for (a) the gas-film mass transfer coefficient k_G and (c) the emission
614 rates J, and the respective field-to-flux hood ratios (b and d). The low wind speed range of (b) and (d) is
615 shown in detail (e) and (f). Legend for (a), (c) and (e) in (a), and for (b), (d) and (f) in (b).
616
617 The procedure summarised in the previous paragraph allows the emission rates of gas-phase controlled
618 compounds measured with the US EPA flux hood to be scaled (at least in order of magnitude) to field
619 conditions different than the mass transfer conditions imposed by the micro-environment inside the flux
620 hood. By back-calculating $C_{G,i}$ using Equation (SM7b), it takes into account the effects of the
621 concentration build-up in the hood`s headspace, which is a feature not present in other proposed scaling
622 methods such as the water evaporative flux ratio correction factor (Parker et al., 2013b) (see discussion
623 in 3.3). The following aspects are important to be observed:
624 • The flux hood has to present a well-mixed headspace, so that Equation (SM7b) is valid, which
625 is the typical case for the US EPA flux hood; for wind tunnel devices, Equation (SM1) shall be
626 used instead, requiring that the bulk gas-phase concentration C_G is known.
627 • Proper recording of the sweep air flow rate Q is necessary for the back-calculation of $C_{G,i}$; this
628 can be done by using calibrated rotameters or in-line electronic flow meters.
629 • If k_G for the desired compound inside the flux hood is to be determined experimentally, the
630 discussion in sub-section 3.2 points out the importance of repetitions and cross-checks in the
631 experiments, to avoid that the k_G retrieved from the experimental results are not significantly
632 affected by the uncertainty in the temperature at the liquid surface and other sources of
633 inaccuracy. Besides, either with k_G determined directly from experiments or calculated based on
634 other compound, it is critical that the operational conditions of the flux hood for which k_G was
635 assessed are as similar as possible to the ones used during the sampling in the field (for instance,

same Q, sampling rate and depth of insertion in the liquid); if scums and slick microfilms are present over the liquid surfaces in the field, this may compromise the reproduction of the conditions.

- The accuracy of the scaling approach is directly dependent on the application of a suitable emission model to approximate the field k_G, and this may vary from case to case.
- The procedure is applicable for scaling emission rates of individual compounds; if the sample is analysed via dynamic olfactometry to obtain odour emission rates, the calculation is not possible, unless the odour is always dominated by a single compound (or group of compounds). As highlighted by Hudson and Ayoko (2008b), since the volatilisation rates of different compounds may respond differently to the mass transfer conditions created by the flux hood, the composition of the odour samples may be altered in relation to the emissions in the absence of the hood, leading, in some cases, to non-representative olfactometry results.

Virtually, the analysis developed in this sub-section could also be adapted to compounds with liquid phase-controlled volatilisation, provided that the value k_L in the area enclosed by the flux hood is known and an appropriate emission model is available to approximate the field situation. However, surface currents are expected to be present in the field (and will vary with the wind speed), and the turbulence arising from the interaction of these currents with the edge of the flux hood will make the mass transfer conditions in the liquid differ from the conditions of the laboratory experiments where the reference k_L for the flux hood is obtained. Moreover, some WWTP units may present bubbling, which can significantly affect the emission rates of more volatile compounds (Grant et al., 2013). For these reasons, we will refrain from extending the complete analysis to liquid phase-controlled compounds. Nonetheless, it is worth mentioning that Rhee et al. (2007), performing experiments in a large wind-wave tank, with size and wind conditions that partially approximate the conditions of the liquid surfaces in a wastewater treatment tank, measured k_L of the order 10^{-5} to 10^{-4} m s^{-1}, for compounds with similar Sc_L as chloroform and H_2S, and friction velocities ranging from 0.09 to 0.61 m s^{-1} (equivalent U_{10} from

662 3.15 to 15.5 m s^{-1}). This means that the k_L observed inside the US EPA flux hood in the absence of
663 surface currents (sub-section 3.2) are one to more than two orders of magnitude lower than the k_L typical
664 of the field.
665
666 **4. CONCLUSIONS**
667
668 The mass transfer inside the US EPA flux hood was assessed by means of experiments of water
669 evaporation and volatilisation of different VOCs, covering different behaviours regarding the dominance
670 of the volatilisation process. Supported by a theoretical analysis, the results were processed in order to
671 obtain the gas-film (k_G) and liquid-film (k_L) mass transfer coefficients in the microenvironment created
672 by the flux hood.
673
674 The VOCs emission rates J and the water evaporation rates J_w generally increased with the sweep air
675 flow rate Q. As expected, at a given Q, J_w was smaller for higher humidity content in the inlet air.
676 Concentration build up in the hood`s headspace was found to significantly affect the mass transfer of
677 compounds whose volatilisation is influenced by the gas phase (acetic acid, 1-butanol and water, in this
678 case), but was not relevant for the compounds with liquid phase-controlled volatilisation (chloroform
679 and H_2S), consistently with the theoretical considerations. Although the water evaporation method
680 (Parker et al., 2013b) is not necessarily applicable to inter-convert between volatilisation rates measured
681 with the US EPA flux hood under different operational conditions, the observed relation between water
682 evaporation and volatilisation rates of acetic acid suggest that the method may be used to approximate
683 relative changes in the magnitude of the volatilisation rate of gas phase-dominated compounds due to
684 changes in Q.
685
686 The mass transfer coefficients for all compounds tended to increase with the sweep air flow rate,
687 reflecting the enhancement of the near-interface turbulence that is expected to occur as Q rises. Due to

688 the difficulty of having accurate values of the temperature at the water surface and an apparent offset in
689 J_w, the calculation of k_G for water vapour directly from the experimental evaporation rates was not
690 possible. However, the values of k_G for acetic acid were shown to be accurate and could be converted
691 using Equation (SM4a) so as to satisfactorily estimate water evaporation rates inside the hood. This
692 highlights the importance of repetitions and cross-checks in the experiments to overcome the challenges
693 inherent to the experimental determination of k_G in a mixed-headspace device such as the US EPA flux
694 hood (affected by concentration build up), such as the uncertainty in the temperature at the liquid surface
695 and in the values of K_H.
696
697 Comparatively, k_G inside the US EPA flux hood under typical operational conditions was found to be
698 of the same order as the respective k_G reported in the literature for wind tunnel-type devices. However,
699 due to the concentration build-up in the flux hood`s headspace (which normally in inexistent or very
700 small in wind tunnels), the emission rates measured by the flux hood may be significantly lower than
701 the emission rates measured by wind tunnels.
702
703 The k_G for acetic acid in the interior of the US EPA flux hood was compared against the k_G calculated
704 by the volatilisation model proposed by Gostelow et al. (2001a) for passive liquid surfaces (adopted here
705 as a proxy for the k_G values in WWTPs, in the absence of the sampling device). This enables the
706 estimation of the magnitude of the potential bias in the emission rate of gas phase-controlled compounds
707 (in this case, acetic acid) introduced by the placement of the flux hood. The k_G in the US EPA flux hood
708 were shown to represent conditions of low wind speeds: for the flow rates of 2, 5 and 10 L min^{-1}, the k_G
709 for acetic acid equal the model estimates for U_{10} = 1.18, 1.25 and 2.36 m s^{-1}, respectively. Nonetheless,
710 because of the concentration build-up in the headspace, J inside the flux hood will be lower than the
711 corresponding emission rates in the field, for the same k_G; for acetic acid, J observed in the flux hood
712 operating with Q = 2, 5 and 10 L min^{-1} are equivalent to the field J for U_{10} = 0.27, 0.51 and 0.99 m s^{-1},

713 respectively. Therefore, measurements of the emission rate of gas phase-controlled compounds made
714 with the US EPA flux hood can be expected to be underestimated for wind speed conditions higher than
715 those (the greater the wind speed, the greater the bias). The general lines of a procedure were devised in
716 order to scale (at least in order of magnitude) the emission rates of gas-phase controlled compounds
717 measured with the US EPA flux hood to field conditions different than the mass transfer conditions
718 imposed by the micro-environment inside the hood. This procedure is subjected to the restrictions
719 highlighted in sub-section 3.3.
720
721 Concerning the liquid-film mass transfer coefficient k_L inside the flux hood, a thorough analysis such as
722 the one made for k_G was not carried out, since the turbulence arising from the interaction of surface
723 currents (which can expected to be present in the field and vary with the wind speed) with the edge of
724 the flux hood will make the k_L inside the flux hood placed in the field differ from the conditions of the
725 laboratory experiments where the reference k_L for the flux hood is obtained. However, as a preliminary
726 estimate, the experimental k_L observed in our study in the US EPA flux hood (absence of surface
727 currents) are one to more than two orders of magnitude lower than the k_L typical of the field (having as
728 reference the experiments of Rhee et al., 2007).
729
730 This is the first time that the mass transfer coefficients (k_G and k_L) for different compounds have been
731 systematically assessed inside the US EPA flux hood under typical operational conditions (Prata Jr. et
732 al., 2016, had previously measured k_L for H_2S with stirring in the liquid phase). The knowledge of the
733 mass transfer coefficients, together with other results reported in this paper, allowed a clear evaluation
734 of this device and a more informed comparison against other enclosure devices. It also could be
735 employed in the estimation of the magnitude of the bias in the emission rate of gas phase-controlled
736 compounds introduced by the placement of the flux hood and in the scaling of the measurements to field
737 conditions, as exemplified. Furthermore, the present results can be used in support and complementarily
738 to CFD studies involving the US EPA flux hood.

ACKNOWLEDGEMENTS

Authors acknowledge the sponsorship from Coordenação de Aperfeiçoamento de Pessoal de Nível Superior (CAPES) and Conselho Nacional de Desenvolvimento Científico e Tecnológico (CNPq), Brazil. The authors also thank Lucas Abreu Gomes for providing practical help during the execution of part of the experiments.

REFERENCES

APHA, AWWA, WEF, 2005. Standard methods for the examination of water and wastewater, 21st ed., American Public Health Association, Washington.

AS/NZS 4323.4:2009. Stationary source emissions Method 4: Area source sampling – Flux chamber technique, Australia/New Zealand Standards.

Beghi S. P., Rodrigues A. C., Sá L. M., Santos J. M., 2012. Estimating hydrogen sulphide emissions from an anaerobic lagoon. Chemical Engineering Transactions 30, 91-96.

Bliss P., Jiang J. K., Schultz T., 1995. The development of a sampling system for the determination of odour emission rate from areal surfaces: II. Mathematical Model. Journal of Air and Waste Management Association, 45, 989-994.

765

766 Blunden J., Aneja V. P., 2008. Characterizing ammonia and hydrogen sulfide emissions from a swine
767 waste treatment lagoon in North Carolina. Atmospheric Environment 42, 3277-3290.

768

769 Capelli L., Sironi S., Del Rosso R., 2013. Odor sampling: techniques and strategies for the estimation of
770 odor emission rates from different source types. Sensors 13, 938-955.

771

772 Capelli L., Sironi S., Del Rosso R., Céntola P., 2009a. Predicting odour emissions from wastewater
773 treatment plants by means of odour emission factors. Water Research 43, 1977-1985.

774

775 Capelli L., Sironi S., Del Rosso R., Céntola P., 2009b. Design and validation of a wind tunnel system
776 for odour sampling on liquid area sources. Water Science and Technology 59 (8), 1611-1620.

777

778 Eckley C. S., Gustin M., Lin C.-J., Li X., Miller M. B., 2010. The influence of dynamic flux chamber
779 design and operating parameters on calculated surface-to-air mercury fluxes. Atmospheric Environment
780 44, 194-203.

781

782 Eklund B., 1992. Practical guidance for flux chamber measurements of fugitive volatile organic emission
783 rates. Journal of the Air & Waste Management Association 42, 1583-1591.

784

785 Gholson A., Albritton J., Jayanty R., 1989. Evaluation of the flux chamber method for measuring volatile
786 organic emissions from surface impoundments. EPA/600/3-89/008, US EPA, Research Triangle Park,
787 North Carolina.

788

789 Gholson A. R., Albritton J. R., Jayanty R. K. M., Knoll J. E., Midgett M. R., 1991. evaluation of an
790 enclosure method for measuring emissions of volatile organic compounds from quiescent liquid
791 surfaces. Environmental Science & Technology 25, 519-524.
792
793 Gostelow P., Longhurst P.J., Parsons S.A., Stuetz R.M., 2003. Sampling for Measurement of Odours.
794 IWA Scientific and Technical Report No. 17, IWA Publishing, London.
795
796 Gostelow, P., Parsons, S. A., Cobb, J. 2001a Development of an odorant emission model for sewage
797 treatment works. Water Sci. Technol. 44 (9), 181–188.
798
799 Gostelow P., Parsons S. A., Stuetz R. M., 2001b Odour measurement in sewage treatment - a review.
800 Water Research 35 (3), 579-597.
801
802 Grant R. H., Boehm M. T., Lawrence A. J., Heber A. J., 2013. Hydrogen sulfide emissions from sow
803 farm lagoons across climates zones. Journal of Environmental Quality 42, 1674-1683.
804
805 Guillot J.-M., Clincke A.-S., Guilleman M., 2014. Odour emission from liquid and solid area sources: a
806 large intercomparison of sampling devices. Chemical Engineering Transactions 40, 151-156.
807
808 Hayes J.E., Stevenson R.J, Stuetz R.M. 2014. The impact of malodour on communities: a review of
809 assessment techniques. Science of the Total Environment, 500-501, 395-407
810
811 Hentz L. H., Murthy S., Mulamula L., Voit K., 2013. Odours emissions relate to operating conditions in
812 a high rate activated sludge treatment process. Proceedings of 5th IWA Specialized Conference on Odors
813 and Air Emissions Jointly Held With 10th Conference on Biofiltration for Air Pollution Control, San
814 Francisco.

Hudson N., Ayoko G. A., 2008a. Odour sampling 1: Physical chemistry considerations. Bioresource Technology 99, 3982-3992.

Hudson N., Ayoko G. A., 2008b. Odour sampling 2: Comparison of physical and aerodynamic characteristics of sampling devices: A review. Bioresource Technology 99, 3993–4007.

Hudson N., Ayoko G. A., 2009. Comparison of emission rate values for odour and odorous chemicals derived from two sampling devices. Atmospheric Environment 43, 3175-3181.

Hudson N., Ayoko G. A., Dunlop M., Duperouzel N., Burrell D., Bell K.; Gallagher E., Nicholas P., Heinrich N., 2009. Comparison of odour emission rates measured from various sources using two sampling devices. Bioresource Technology 100, 118-124.

Jiang J. K., Bliss P., Schultz T., 1995. The development of a sampling system for the determination of odour emission rate from areal surfaces: I. Aerodynamic performance. Journal of Air and Waste Management Association 45, 917-922.

Jiang, K., Kaye, R., 1996. Comparison study on portable wind tunnel system and isolation chamber for determination of VOC's from areal sources. Water Science and Technology 34 (3-4), 583-589.

Klenbusch M., 1986. Measurement of gaseous emission rates from land surfaces using an emission isolation flux chamber. US EPA, Environmental Monitoring Systems Laboratory, Las Vegas.

839 Leyris C., Guillot J.-M., Fanlo J.-L., Pourtier L., 2005. Comparison and development of dynamic flux
840 chambers to determine odorous compound emission rates from area sources. Chemosphere 59 (3), 415-
841 421.
842
843 Lin C.-J., Zhu W., Xianchang L., Xinbin F., Sommar J., Shang L., 2012. Novel dynamic flux chamber
844 for measuring air-surface exchange of Hg^0 from soils. Environmental Science & Technology 46, 8910-
845 8920.
846
847 Lucernoni F., Rizzotto M., Tapparo F., Capelli L., Sironi S., Busini V., 2016. Use of CFD for static
848 sampling hood design: An example for methane flux assessment on landfill surfaces. Chemosphere 163,
849 259-269.
850
851 Lucernoni F., Capelli L., Busini V., Sironi S., 2017. A model to relate wind tunnel measurements to
852 open field odorant emissions from liquid area sources. Atmospheric Environment 157, 10-17.
853
854 Muezzinoglu A., 2003. A study of volatile organic sulfur emissions causing urban odors. Chemosphere
855 51, 245-252.
856
857 Nicell J. A., 2009. Assessment and regulation of odour impacts. Atmospheric Environment 43, 196-206.
858
859 Parker D. B., Caraway E., Rhoades M., Donnell C., Spears J., Cole N. A., Todd R., Casey K. D. 2008
860 Effect of Wind Tunnel Air Velocity on VOC Flux Rates from CAFO Manure and Wastewater. ASABE
861 Paper No. 083897. St. Joseph, Mich.: ASABE.
862

Parker D., Gilley J., Woodbury B., Kim K.-H., Galvin G., Bartelt-Hunt S., Li X., Snow D., 2013a. Odorous VOC emission following land application of swine manure slurry. Atmospheric Environment 66, 91-100.

Parker D., Ham J., Woodbury B., Cai L., Spiehs M., Rhoades M., Trabue S., Casey K., Todd R., Cole A., 2013b. Standardization of flux chamber and wind tunnel flux measurements for quantifying volatile organic compound and ammonia emissions from area sources at animal feeding operations. Atmospheric Environment 66, 72-83.

Prata Jr., A.A., Santos, J.M., Beghi, S.P., Fernandes, I.F., Vom Marttens, L.L.C., Neto, L.P., Martins, R.S., Reis Jr., N.C., Stuetz, R.M., 2016. Dynamic flux chamber measurements of hydrogen sulfide emission rate from a quiescent surface: a computational evaluation. Chemosphere 146, 426-434.

Prata Jr. A. A., Santos J. M., Timchenko V., Stuetz R. M., 2014. Use of computational fluid dynamics in the analysis of a portable wind tunnel for sampling of odorous emissions at liquid surfaces. Chemical Engineering Transactions 40, 145-150.

Rhee T. S., Nightingale P. D., Woolf D. K., Caulliez G., Bowyer P., Andreae M. O. 2007. Influence of energetic wind and waves on gas transfer in a large wind–wave tunnel facility. Journal of Geophysical Research, 112, C05027.

Rhoades, M., Parker, D., Cole, N., DeOtte, R., Auvermann, B., Buser, Z., 2005. Factors affecting ammonia emission measurements with surface isolation flux chambers. In: Proceedings Annual International Meeting of the American Society of Agricultural and Biological Engineers. ASABE Paper No. 05-4026. July 17-20. Tampa, FL, USA.

889 Rumsey I. C., Aneja V. P., Lonneman W. A., 2012. Characterizing non-methane volatile organic
890 compounds emissions from a swine concentrated animal feeding operation. Atmospheric Environment
891 47, 348-357.
892
893 Saha C. K., Wua W., Zhang G., Bjerg B., 2011. Assessing effect of wind tunnel sizes on air velocity and
894 concentration boundary layers and on ammonia emission estimation using computational fluid dynamics
895 (CFD). Computers and Electronics in Agriculture 78, 49-60.
896
897 Sander, R., 2015. Compilation of Henry's law constants (version 4.0) for water as solvent. Atmospheric
898 Chemistry & Physics 15, 4399-4981.
899
900 Santos J. M., Kreim V., Guillot J.-M., Reis Junior N. C., Sá L. M., Horan N. J., 2012. An experimental
901 determination of the H_2S overall mass transfer coefficient from quiescent surfaces at wastewater
902 treatment plants. Atmospheric Environment 60, 18-24.
903
904 Schauberger, G., Piringer, M., Baumann-Stanzer, K., Knauder, W., Petz, E. 2013 Use of a Monte Carlo
905 technique to complete a fragmented set of H_2S emission rates from a wastewater treatment plant. Journal
906 of Hazardous Materials 263, 694-701.
907
908 Smith, S. D. 1980 Wind stress and heat flux over the ocean in gale force winds. J. Phys. Oceanogr. 10,
909 709–726.
910
911 Sohn J. H., Smith R. J., Hudson N. A., Choi H. L., 2005. Gas sampling efficiencies and aerodynamic
912 characteristics of a laboratory wind tunnel for odour measurement. Biosystems Engineering 92 (1), 37-
913 46.
914

915 Wang X., Jiang J., Kaye R., 2001. Improvement of a wind-tunnel sampling system for odour and VOCs.
916 Water Science and Technology 44 (9), 71-77.
917
918 Wang B., Sivret E. C., Parcsi G., Stuetz R. M., 2015. Determination of VOSCs in sewer headspace air
919 using TD–GC–SCD. Talanta 137, 71-79.
920
921 Woodbury B. L., Parker D. B., Eigenberg R. A., Spiehs, M. J., 2011. Flow characteristics of a dynamic
922 EPA flux chamber. Proceedings of 2011 Annual International Meeting of the American Society of
923 Agricultural and Biological Engineers, ASABE Paper No. 11-11096, Louisville, KY, USA.
924
925 Xiao S., Yang H., Liu D., Zhang C., Lei D., Wang Y., Peng F., Li Y., Wang C., Li X., Wu G., Liu L.
926 2014. Gas transfer velocities of methane and carbon dioxide in a subtropical shallow pond. Tellus B 66,
927 23795.
928